

EFFECT OF HIGH-FREQUENCY DISTRIBUTED FORCING ON THE TURBULENCE CASCADE IN THE WAKE OF A BLUNT TRAILING EDGE BODY

Ross Cruikshank & Philippe Lavoie

Institute for Aerospace Studies

University of Toronto

4925 Dufferin St., Toronto, Ontario, M3H 5T6, Canada

ross.cruikshank@mail.utoronto.ca & lavoie@utias.utoronto.ca

ABSTRACT

High-frequency forcing is applied with an array of synthetic jet actuators to manipulate the large and small scale motions in the wake of a blunt trailing edge profiled body at $Re = 2500$. Forcing causes an increase in the energy of the random motions in the shear layer, a higher dissipation rate of turbulent kinetic energy, and attenuates the coherent large scale velocity fluctuations. The reduced strength of the shear layers under forced conditions is linked to a significantly weaker vortex street in a plane closely aligned to the centerline of the jets. The coupling between the small scales that are acted upon by the forcing and the large scales of the flow is investigated using a generalized scale-by-scale energy balance with the Kármán-Howarth-Monin-Hill equation. This shows that the turbulence cascade is significantly altered by the high-frequency forcing, accelerating the interscale cascade from large to small scales in the shear layer, and diminishing inverse cascading behavior at large scales along the wake centerline.

INTRODUCTION

Manipulation of the separated shear layers of a bluff body can have a considerable effect on the resulting large scale vortical structures that develop in the wake and consequently reduce the drag. One methodology to effectively control the evolution of a shear layer is to excite it at the most receptive frequencies of coherent structures (Ho & Huerre, 1984). This type of periodic forcing typically involves the generation of relatively large scale vortices which can increase the rate of entrainment in the shear layer (Dandois *et al.*, 2007). If this approach is applied to a flow with a global instability such as a vortex street, there is a risk in amplifying the instability or triggering other instability modes. An alternate approach to control the large scales of a flow is to introduce small scale vortices which are decoupled from the dominant base flow instabilities. With this methodology, the forcing can reduce the amplitude of the velocity fluctuations by increasing the dissipation, stabilizing the shear layer and reducing the entrainment rate (Vukasinovic *et al.*, 2010; Cain *et al.*, 2001). Wiltse & Glezer (1998) further observed that actuation at the small scales of a free shear layer caused significant modifications to the overall energy cascade, amplifying the high frequency content and diminishing the low frequency energy, which they associated with an acceleration of the energy

transfer from the large to small scales. The effectiveness of high-frequency forcing has been demonstrated in flow control applications such as the wake of an axisymmetric bluff body by Oxlade *et al.* (2015), who measured a base pressure recovery of 35% due to the reduced entrainment from the weaker forced shear layers, and separation control on an airfoil by Glezer *et al.* (2005), who observed a drop in coherent flow oscillations.

The present study further investigates the effect of high-frequency forcing on the large and small scales in the wake of a blunt trailing edge (BTE) profiled body. In order to investigate the effect on the energy cascade, the Kármán-Howarth-Monin-Hill (KMH) equation is employed (Hill, 2002). The KMH equation describes the generalized scale-by-scale energy budget for the second order structure function $\langle \delta q^2 \rangle = \langle \delta u_i \delta u_i \rangle$, where $\delta u_i = u_i^+ - u_i^-$ is the fluctuating velocity difference between $x_i^+ = x_i + \vec{r}_i/2$ and $x_i^- = x_i - \vec{r}_i/2$, x_i refers to a point in physical space and \vec{r}_i is a vector denoting an orientation and separation in scale space. Adopting the notation of Portela *et al.* (2017), the KMH equation is given by

$$\begin{aligned} \frac{\partial \langle \delta q^2 \rangle}{\partial t} + \frac{\partial \frac{u_i^+ + u_i^-}{2} \langle \delta q^2 \rangle}{\partial x_i} + \frac{\partial \langle \delta u_i \delta q^2 \rangle}{\partial r_i} + \frac{\partial \delta U_i \langle \delta q^2 \rangle}{\partial r_i} = \\ (1) \\ - 2 \langle \delta u_i \delta u_j \rangle \frac{\partial \delta U_j}{\partial r_i} - \langle (u_i^+ + u_i^-) \delta u_j \rangle \frac{\partial \delta U_j}{\partial x_i} \\ - \frac{\partial \left\langle \frac{u_i^+ + u_i^-}{2} \delta q^2 \right\rangle}{\partial x_i} - 2 \frac{\partial \langle \delta u_i \delta p \rangle}{\partial x_i} + \nu \frac{1}{2} \frac{\partial^2 \langle \delta q^2 \rangle}{\partial x_i \partial x_i} \\ + 2\nu \frac{\partial^2 \langle \delta q^2 \rangle}{\partial r_i \partial r_i} - 4\nu \left(\left\langle \frac{\partial \delta u_j}{\partial x_i} \frac{\partial \delta u_j}{\partial x_i} \right\rangle + \frac{1}{4} \left\langle \frac{\partial \delta u_j}{\partial r_i} \frac{\partial \delta u_j}{\partial r_i} \right\rangle \right) \end{aligned}$$

where the terms are represented symbolically as

$$\mathcal{A}_i = -\mathcal{A} - \Pi - \Pi_U + \mathcal{P} + \mathcal{T}_u + \mathcal{T}_p + \mathcal{D}_x + \mathcal{D}_r - \varepsilon_r$$

describing advection (\mathcal{A}), nonlinear interscale energy transfer (Π), linear interscale energy transfer (Π_U), production (\mathcal{P}), transport from turbulent fluctuations (\mathcal{T}_u), transport from velocity/pressure correlations (\mathcal{T}_p), diffusion in physical and scale space ($\mathcal{D}_x, \mathcal{D}_r$), and the dissipation rate (ε_r).

METHODOLOGY

The wake of a blunt trailing edge (BTE) model of thickness $d = 25.4$ mm, shown in Figure 1, is experimentally examined. The model was installed inside an open-circuit suction tunnel with a cross-section of 0.3 m by 0.3 m and a fixed Re of 2500 was considered, generating a laminar boundary layer with a momentum thickness $\theta = 0.038d$ at the trailing edge. High-frequency forcing was provided by an array of piezoelectric-driven synthetic jets. The jets used in the experiments feature rectangular slot exits $1.2d$ long with aspect ratios of 38, and are oriented spanwise relative to the crossflow. They are located on both sides of the BTE body ($c/d = 12.9$), $1.05d$ upstream of the trailing edge, and are spaced apart by $2.4d$. This matches the spanwise wavelength of the Mode B' secondary instability of the vortex street, as identified by Naghib-Lahouti *et al.* (2014). The jets were individually calibrated by measuring their output velocity at the slot exit plane with a hot wire in the absence of a crossflow. The forcing amplitude of the synthetic jets was assessed with the velocity ratio, $R = \frac{1}{T/2} \int_0^{T/2} u_j(t) dt / u_\infty$, where T is the cycle period, $u_j(t)$ is the measured jet velocity, and the integral was only evaluated over the blowing stroke. The effect of forcing at $R = 6.2$ and $R = 8$ will be examined in this paper. These cases were selected because $R = 6.2$ is around the maximum forcing amplitude at this Re for which the vortical structures emitted by the jets remained inside the boundary layer. The jets were operated at a frequency of 2000 Hz, which is an order of magnitude above the shedding and shear layer instability frequencies.

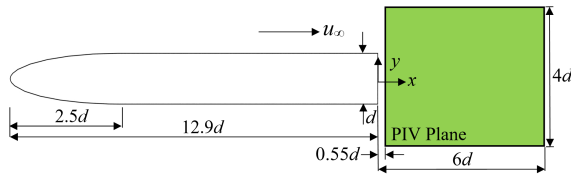


Figure 1: Schematic of the blunt trailing edge model and the field of view of the x - y PIV plane.

The velocity field in the x - y plane, spanwise offset by $z = 0.08d$ from the centerline of a jet, was measured using stereo-PIV. The PIV setup consisted of a 1 mm thick laser sheet formed from a dual-pulse Nd-YAG laser, and two Lavision sCMOS cameras positioned roughly symmetrically at 40° angles on opposite sides of the wind tunnel. Both cameras had 60 mm focal length lenses. The field of view extended from $0.55d < x < 6d$ and $-2d < y < 2d$. For every case 1560 random snapshots were taken at a frequency of approximately 2 Hz. The snapshots were processed using Lavision Davis 8.3.x software with a window size of 16×16 pixels and 50% overlap, resulting in a vector spacing of $0.02d$. The Kolomogorov lengthscale $\eta = (\nu^3/\bar{\epsilon})^{1/4}$, estimated by computing the mean dissipation rate of TKE $\bar{\epsilon}$, is about $0.01d$ in the near wake, suggesting that this vector spacing is sufficient to resolve the small scales of the flow at this Re (Lavoie *et al.*, 2007).

In its complete form $\bar{\epsilon}$ can be calculated from the 9 velocity gradients from all spatial directions:

$$\bar{\epsilon} = -\nu \overline{\frac{\partial u_i}{\partial x_j} \left(\frac{\partial u_i}{\partial x_j} + \frac{\partial u_j}{\partial x_i} \right)} \quad (2)$$

With stereo-PIV in the x - y plane, only 6 of the fluctuating velocity gradients are directly measurable: $\partial u/\partial x$, $\partial v/\partial x$, $\partial w/\partial x$, $\partial u/\partial y$, $\partial v/\partial y$, and $\partial w/\partial y$. The remaining 3 velocity gradients are approximated using an isotropic assumption, namely, $\partial u/\partial z \approx \partial u/\partial y$, $\partial v/\partial z \approx \partial v/\partial y$, and $\partial w/\partial z \approx 0.5(\partial u/\partial x + \partial v/\partial y)$.

Hot-wire measurements were taken using a Dantec StreamLine constant-temperature anemometer, sampled at 25 kHz and low pass filtered at 10 kHz for a typical sampling time of 60 s. The hot-wires were custom-made on a Dantec probe with $5 \mu\text{m}$ thick tungsten wire to have a sensing length of about 1 mm.

RESULTS AND DISCUSSION

High-frequency forcing can significantly modify how the spectral energy is distributed in a flow. The effect of forcing on the velocity spectra at $\{x = 0.2d, y = 0.53d\}$ is shown in Figure 2. In the unforced case, the dominant frequency component is at $fd/u_\infty = 0.25$, corresponding to the vortex shedding instability. Higher order harmonics of the shedding frequency, as well as the shear layer instability frequency at $fd/u_\infty = 1.34$ are also evident. With both levels of forcing, these spectral peaks are completely suppressed at this measurement location, but the energy throughout the entire spectra is increased except at the instability frequency, resulting in an overall increase in the velocity fluctuations. In the forced spectra, the peak at the forcing frequency is higher than any other frequency component. A clear peak at the forcing frequency can be identified in the velocity spectra throughout the near wake region, presumably because of the advection of the vortices generated by the jets into the wake as well as acoustic-related coupling effects. Interestingly, at $\{x = 0.2d, y = 0.53d\}$ the forcing frequency peak is greater for the $R = 6.2$ case compared to the $R = 8$ case, which may be linked to the higher penetration of the jet into the freestream in the higher forcing amplitude case. Additionally, while the energy at intermediate scales is very similar at $R = 6.2$ and $R = 8$, the low frequencies are amplified more for $R = 8$. The amplification of the incoherent low frequency energy content by high-frequency forcing in the present study stands in contrast to previous studies such as Wiltse & Glezer (1998) and Vukasinovic *et al.* (2010), which report a diminution of large scale energy from the forcing of free shear layers and backward facing step flows, respectively. This discrepancy may be because in the aforementioned studies the unforced shear layer was fully turbulent and did not feature a global instability. However, the attenuation of the shedding instability in the present study is still indicative of a coupling between the small scales that are acted upon by the forcing and the large scale features of the wake.

In order to examine the effect of forcing of the small-scales on the large scale vortex street, a triple decomposition of the total wake velocity field in the x - y plane was employed to isolate the mean, the vortex shedding induced periodic fluctuations, and the random fluctuations. In this study, the reference for the shedding cycle was obtained using the snapshot proper orthogonal decomposition (POD)

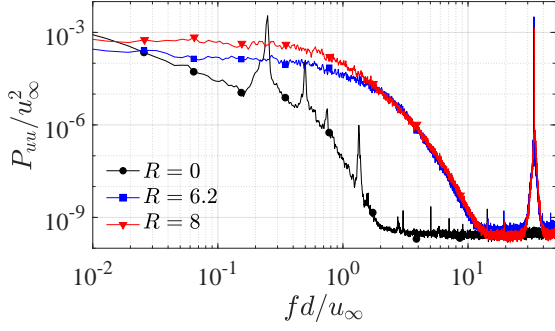


Figure 2: Velocity PSD at $\{x = 0.2d, y = 0.53d\}$ unforced and with forcing at $R = 6.2$ and $R = 8$.

based method of van Oudheusden *et al.* (2005) rather than from a time-resolved reference signal. The snapshots were sorted into 18 phase bins, which translates to roughly 85 snapshots per bin. Conditionally averaged statistics with respect to the vortex shedding phase are denoted with a tilde.

The spanwise vorticity fields at a selected phase for the unforced, and the $R = 6.2$ and $R = 8$ forcing cases in the $z = 0.08d$ plane are presented in Figure 3. In the unforced case, a well-organized vortex street originating from the separated shear layers is revealed. In the forced cases, the shear layers are more spread across both the base and freestream side of the flow due to the upwash of low momentum fluid in this plane. In the $R = 8$ case in particular, where the jet fully penetrates the boundary layer and the flow reverses downstream of the jet slot, two distinct regions in the shear layer are created: an inner region with a comparatively greater velocity gradient, and an outer region with a much lower velocity gradient where the velocity reaches the freestream. As a result, extra inflection points in the velocity profile are created which may have the potential to trigger additional instabilities in the flow. To measure the length scale of the (mean) shear layer, the integral thickness, θ , was computed as

$$\theta = \int \frac{\bar{U} - \bar{U}_{\min}}{\bar{U}_{\max} - \bar{U}_{\min}} \left(1 - \frac{\bar{U} - \bar{U}_{\min}}{\bar{U}_{\max} - \bar{U}_{\min}} \right) dy \quad (3)$$

where \bar{U}_{\max} and \bar{U}_{\min} are the maximum and minimum mean velocities across the shear layer. At the upstream edge of the PIV measurement window ($x = 0.55d$), $\theta = 0.066d$ without forcing, and increases to $0.075d$ for $R = 6.2$ and $0.14d$ for $R = 8$ (with respect to the upper shear layer). The thickening of the shear layers and the corresponding reduction in the intensity of the spanwise vorticity inside them inhibits their interaction, resulting in weaker vortex shedding. In particular, at $x = 4d$ the circulation contained inside the shed vortices is about 60% of the unforced value for the $R = 6.2$ case and 50% for the $R = 8$ case. The reduced strength and more diffuse organization of the shed vortices under forced conditions is clearly evident in Figure 3, and is consistent with the diminished peak in the velocity PSD at the shedding frequency. In the $R = 8$ case, the shed vortices are weaker than in the $R = 6.2$ case because they initially form from only the inner part of the shear layers, effectively reducing the available circulation flux. However, by $x \approx 3d$ the outer shear layers start to move towards the wake centerline and the fluid is entrained into the the von Kármán

vortices, causing the vortices to grow. Further increasing R shifts this entrainment farther downstream, but even at R as high as 10.5, the vortex street is never entirely decimated with the present forcing strategy, and the resulting increase in the width of the wake at these relatively high forcing amplitudes mitigates the drag reduction.

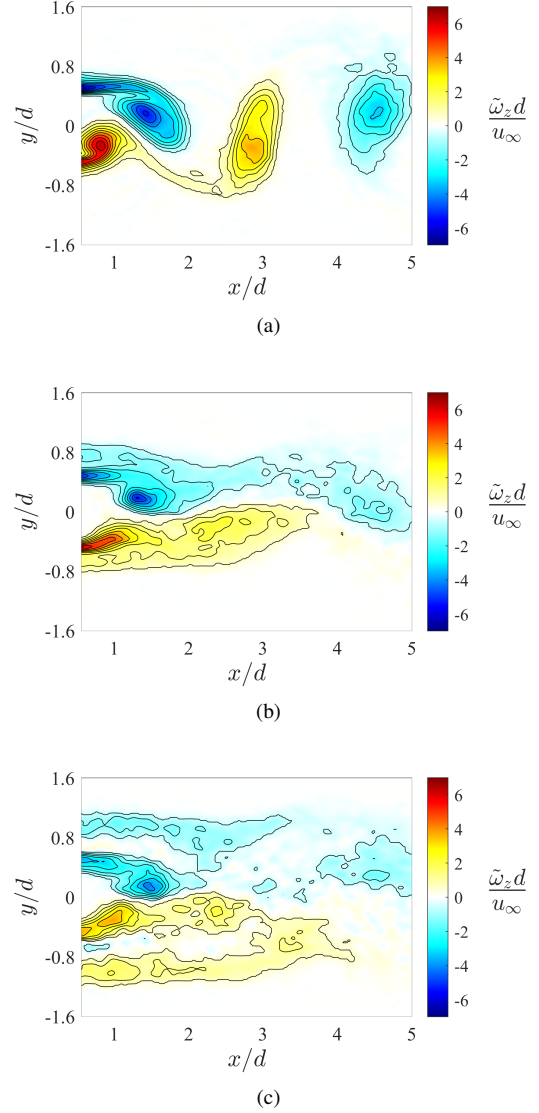


Figure 3: Phase averaged spanwise vorticity in the $z = 0.08d$ plane. (a) Unforced, (b) $R = 6.2$, (c) $R = 8$.

As suggested by the velocity PSD shown in Figure 2, high-frequency forcing and the corresponding attenuation of the vortex street effect also impacts the turbulent properties of the wake. The turbulent kinetic energy (TKE), $\bar{k} = 0.5(\overline{u'u'} + \overline{v'v'} + \overline{w'w'})$, in the wake with and without forcing is plotted in Figure 4. In the forced wake, the induced flow from the jets causes a significant initial increase in the TKE inside and at the freestream side of the shear layers, which is followed by a damping of the TKE downstream. An initial increase of TKE followed by a drop to below the unforced level using high-frequency forcing was previously reported by Dandois *et al.* (2007) and Vukasinovic *et al.* (2010). In the present case, the drop in the total TKE is due to the reduction in the coherent vortex shedding component, which

is evident from the triple decomposition of the velocity fluctuations but is not shown explicitly here for brevity. In both the forcing cases, the coherent component of the velocity fluctuations in the shear layers is diminished to a similar extent, but in the $R = 8$ case, the random fluctuations are approximately double the $R = 6.2$ case at $x = 0.55d$. As a result, the point at which the total TKE drops below the unforced level occurs farther downstream, $x = 0.85d$, compared to $x = 0.65d$. Furthermore, the triple decomposition of the velocity fluctuations shows that the decrease in the total TKE along the wake centerline in both the forced cases is also because of the vortex street attenuation, and that the random component of the fluctuations is actually increased. This observation is in line with an accelerated transfer of energy from the large scale wake instability to the smaller scales by high-frequency forcing. Since the dissipation rate in a flow is proportional to the frequency squared, it may also be expected that the increase in the energy at high frequencies by forcing will be associated with enhanced dissipation of TKE.

The importance of the mean turbulence dissipation rate, $\bar{\epsilon}$, to the changes in the TKE distribution with high-frequency forcing has previously been emphasized in studies such as Wiltse & Glezer (1998), Glezer *et al.* (2005) and Vukasinovic *et al.* (2010). Figure 5 presents $\bar{\epsilon}$ in the $z = 0.08d$ plane with and without forcing. Without forcing, $\bar{\epsilon}$ peaks near the end of the vortex formation region, roughly corresponding to the location where the shear layers roll up into the vortex street. Due to the high-frequency forcing $\bar{\epsilon}$ is about 3 times greater in this region, coinciding with the decreased overall TKE and increased random (small scale) energy. The dissipation is also significantly higher throughout the forced shear layers due to the advection of the small scale vortices generated by the forcing into the wake along and around the freestream side of the shear layers. Furthermore, because the random fluctuations are greater in the $R = 8$ case compared to at $R = 6.2$, $\bar{\epsilon}$ is also correspondingly larger. The advection of the small scale vortices emitted by the jets from the shear layers into the shed von Kármán vortices suggests that the small scales may be linked to the evolution of the large scale wake features.

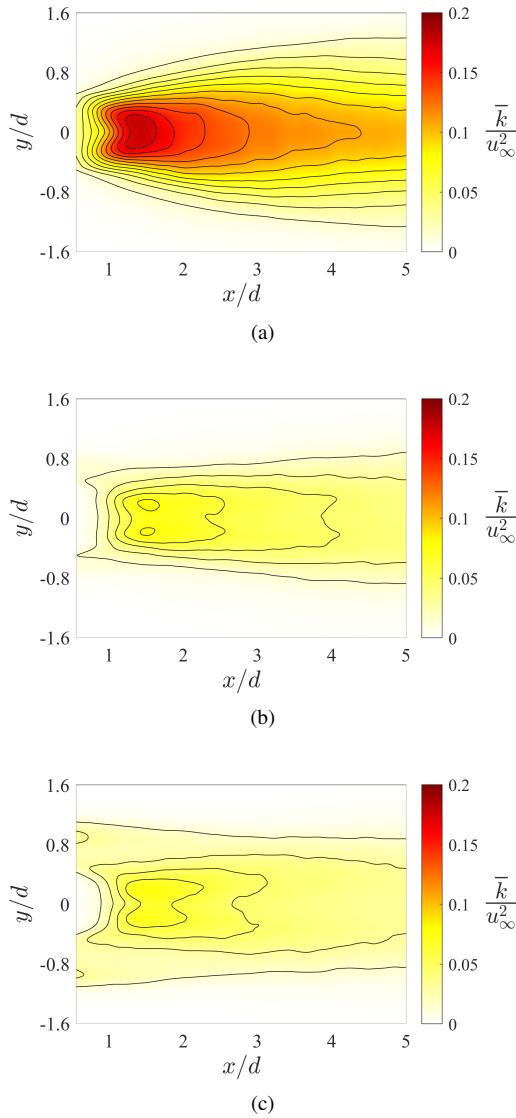


Figure 4: TKE in the $z = 0.08d$ plane. (a) Unforced, (b) $R = 6.2$, (c) $R = 8$.

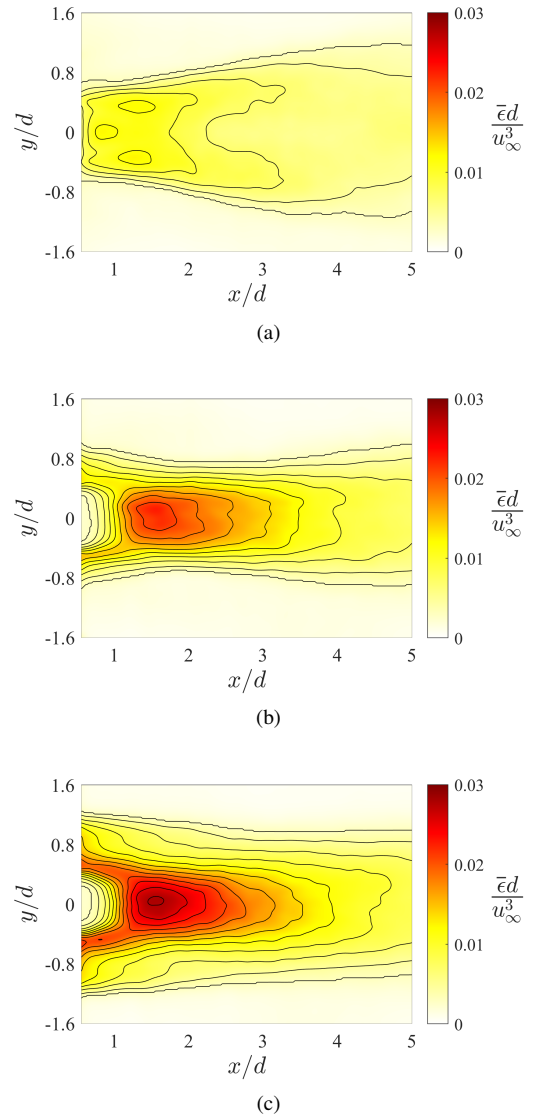


Figure 5: The mean dissipation rate of TKE in the $z = 0.08d$ plane. (a) Unforced, (b) $R = 6.2$, (c) $R = 8$.

In order to better understand the coupling between the large and small scale structures in the wake under high-frequency forcing, the energy cascade is examined using Equation 1. We are restricting our attention here to the unforced and $R = 6.2$ case for simplicity. Structure function terms that could not be directly calculated from the x - y plane stereo-PIV measurements were estimated using an isotropic assumption (for the fluctuating velocity difference terms) similarly to the dissipation in Equation (2), and mean velocity differences in the z direction were neglected. The pressure transport term in Equation 1 was calculated from the remainder of the other terms in the scale-by-scale energy budget, similarly to Gomes-Fernandes *et al.* (2015). The calculated quantities at a particular location in physical space, $\{x, y, z\}$, were interpolated onto a cylindrical coordinate system in the x - y plane in scale space, which is a function of the scale, r_i , and angle, ϕ . The reader is encouraged to refer to Gomes-Fernandes *et al.* (2015) and Portela *et al.* (2017) for a more complete discussion on the individual terms in Equation 1 and the assumptions involved in evaluating them from planar PIV.

While a full analysis of every term in Equation 1 is beyond the scope of this paper, we choose to focus on the net interscale energy transfer, $(-\Pi - \Pi_U)$, to analyze the effect of forcing on the coupling between the large and small scales. The distribution of the sum of these terms, normalized by the dissipation in scale space at $\{x = 1.1d, y = 0.5d, z = 0.08d\}$ with and without forcing is plotted in Figure 6. This location is the most upstream point in the shear layer for which the energy transfer at scales up to $1d$ can be computed. A region of positive (negative) $(-\Pi - \Pi_U)$ is indicative of a forward (inverse) cascade behavior. In a classical Kolmogorov cascade, the interscale energy transfer would be equal to the dissipation rate over a wide range of scales. However, in both the unforced and forced cases at $\{x = 1.1d, y = 0.5d, z = 0.08d\}$, the distributions of $(-\Pi - \Pi_U)$ are highly anisotropic and stratified along the r_2 axis. Additionally, in both cases there is a combination of forward and inverse cascade behaviors at different orientations. To determine the net direction of the energy cascade between scales, the orientation average (in the measured plane) of the terms in Equation 1 was calculated, as in, for example $\Pi^a(r) = (1/2\pi) \int_0^{2\pi} \Pi(r, \phi) d\phi$. The orientation-averaged scale-by-scale energy budget at $\{x = 1.1d, y = 0.5d, z = 0.08d\}$ can be constructed by evaluating the other terms in Equation 1, resulting in Figure 7. The dashed black line corresponds to the sum of the plotted terms, and always equals 1 because \mathcal{T}_p was calculated from the difference of the other terms. Without forcing, at this location in the shear layer the energy budget reveals that the production and advection terms dominate the large scale behavior, and from about $0.1d < r_i < 0.6d$ there is a net inverse cascading behavior. Forcing alters the cascade at this location, reducing the relative importance of advection in the scale-by-scale energy budget and leading to an overall forward cascading behavior across all scales. This is consistent with the breakdown of the large scale vortex shedding structure to smaller scales by forcing.

The energy budget varies dramatically in space, reflecting the inhomogeneity of the near wake. To efficiently map the effect of forcing on the net interscale energy transfer throughout the near wake, Equation 1 was evaluated across a grid of locations in physical space. The distribution of $(-\Pi^a - \Pi_U^a)$ at $r_i = 0.1d$ (small scales) and $r_i = 1d$ (large scales) in the unforced and forced cases are shown in Fig-

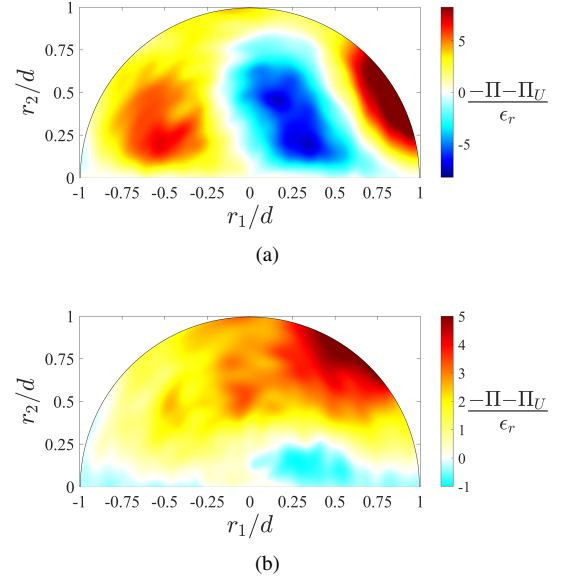


Figure 6: Distribution of $(-\Pi - \Pi_U)/\epsilon_r$ in scale space at $\{x = 1.1d, y = 0.5d, z = 0.08d\}$: (a) Unforced, (b) $R = 6.2$.

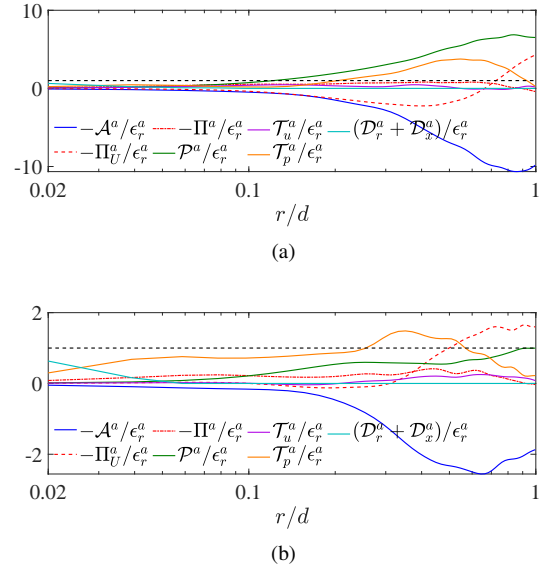


Figure 7: Orientation-averaged scale-by-scale energy budget using Equation 1 at $\{x = 1.1d, y = 0.5d, z = 0.08d\}$: (a) Unforced, (b) $R = 6.2$.

ure 8. At small scales, the net interscale energy in the shear layer is similar in both the unforced and forced cases. With forcing, the interscale energy transfer at small scales is notably increased along the wake centerline, which may be related to the higher TKE dissipation rate along the wake centerline due to the generated small scale vortices. At large scales, the net interscale energy transfer has an inverse behavior at the vortex formation region and up to $x \approx 4d$ due to the growth of the vortex street. The attenuation of the vortex street by forcing reduces this inverse cascading behavior considerably. Therefore, the findings of this study reinforce the fact that high-frequency forcing can attenuate a global flow instability, such as vortex shedding, and significantly modify the entire turbulence cascade despite directly acting

only on the small scales of the flow.

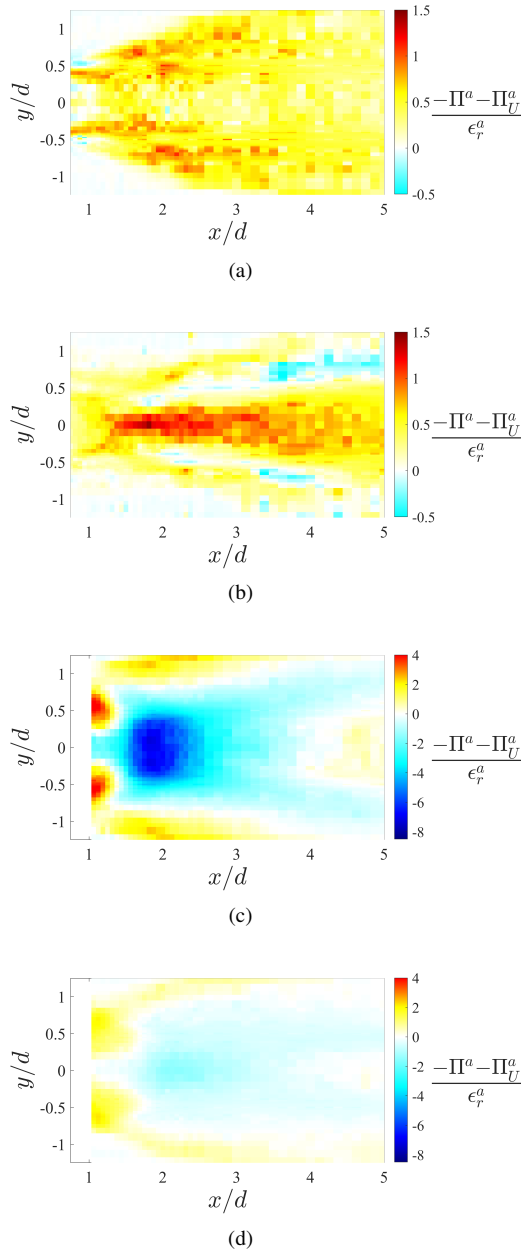


Figure 8: Distribution of $(-\Pi^a - \Pi_U^a)/\varepsilon_r^a$ throughout the near wake at small and large scales. (a) Unforced, $r_i = 0.1d$; (b) $R = 6.2, r_i = 0.1d$; (c) Unforced, $r_i = 1d$; (d) $R = 6.2, r_i = 1d$.

CONCLUSION

The small and large scale behavior of the wake of a blunt trailing edge body at $Re = 2500$ was altered by high-frequency forcing. Direct excitation of the small scales of the flow was achieved using an array of spanwise-oriented synthetic jets operating at a frequency more than an order of magnitude greater than the dominant instability frequencies of the base flow. Forcing was applied upstream of the trailing edge at two different amplitudes, generating small

scale vortices which were convected along and outside of the shear layers into the forming vortex street. This significantly increased the dissipation rate of TKE in the shear layers and wake, which was accompanied by higher random velocity fluctuations but diminished low-frequency coherent fluctuations. Phase averaging of the wake velocity field showed that in the $z = 0.08d$ measurement plane the interaction of the separated shear layers was inhibited due to their increased thickness and reduced strength. While forcing did not entirely decimate the vortex street, the strength of the shed vortices was reduced by about 50%. The effect of forcing on the interscale energy transfer in the turbulence cascade was examined using Equation 1. It showed that at intermediate length scales in the shear layer, the energy transfer from large to small scales was accelerated. Furthermore, the attenuation of the vortex street by forcing was linked to diminished inverse cascading behavior at large scales along the wake centerline. These results echo previous studies that high-frequency forcing is capable of coupling to the large scales in a flow, allowing for effective control of global instabilities such as vortex shedding.

REFERENCES

- Cain, A., Rogers, M., Kibens, V. & Raman, G. 2001 Simulations of high-frequency excitation of a plane wake. In *AIAA 39th Aerospace Sciences Meeting and Exhibit, Aerospace Sciences Meetings*. Reno, NV, AIAA Paper 2001-0514.
- Dandois, J., Garnier, E. & Sagaut, P. 2007 Numerical simulation of active separation control by a synthetic jet. *J. Fluid Mech.* **574**, 25–58.
- Glezer, A., Amitay, M. & Honohan, A. 2005 Aspects of low and high-frequency actuation for aerodynamic flow control. *AIAA J.* **43** (7), 1501–1511.
- Gomes-Fernandes, R., Ganapathisubramani, B. & Vassilicos, J. 2015 The energy cascade in near-field non-homogeneous non-isotropic turbulence. *J. Fluid Mech.* **771**, 676–705.
- Hill, R. 2002 Exact second-order structure-function relationships. *J. Fluid Mech.* **468**, 317–326.
- Ho, C. & Huerre, P. 1984 Perturbed free shear layers. *Ann. Rev. Fluid Mech.* **16**, 365–424.
- Lavoie, P., Avallone, G., De Gregorio, F., Romano, G.P. & Antonia, R.A. 2007 Spatial resolution of PIV for the measurement of turbulence. *Exp. Fluids* **43**, 39–51.
- Naghieb-Lahouti, A., Lavoie, P. & Hangan, H. 2014 Wake instabilities of a blunt trailing edge profiled body at intermediate reynolds numbers. *Exp. Fluids* **55**.
- van Oudheusden, B., Scarano, F., van Hinsberg, N.P. & Watt, D.W. 2005 Phase-resolved characterization of vortex shedding in the near wake of a square-section cylinder at incidence. *Exp. Fluids* **39**, 86–98.
- Oxlade, A., Morrison, J., Qubain, A. & Rigas, G. 2015 High-frequency forcing of a turbulent axisymmetric wake. *J. Fluid Mech.* **770**, 305–318.
- Portela, F., Papadakis, G. & Vassilicos, J. 2017 The turbulence cascade in the near wake of a square prism. *J. Fluid Mech.* **825**, 315–352.
- Vukasinovic, B., Rusak, Z. & Glezer, A. 2010 Dissipative small-scale actuation of a turbulent shear layer. *J. Fluid Mech.* **656**, 51–81.
- Wiltse, J. & Glezer, A. 1998 Direct excitation of small-scale motions in free shear flows. *Phys. Fluids* **8**, 2026–2036.